

11 **Abstract**

12 Ammonia (NH₃) is an important air pollutant which, as precursor of fine particulate matter, raises
13 public health issues. This study analyzes 2.5-years of NH₃ observations derived from ground-based
14 (miniDOAS) and satellite (IASI) remote sensing instruments to quantify, for the first time, temporal
15 variabilities (from interannual to diurnal) of NH₃ concentrations in Paris.

16 The IASI and miniDOAS datasets are found to be in relatively good agreement ($R>0.70$) when
17 atmospheric NH₃ concentrations are high and driven by regional agricultural activities. Over the
18 investigated period (January 2020 – June 2022), NH₃ average concentrations in Paris measured by the
19 miniDOAS and IASI are 2.23 $\mu\text{g}\cdot\text{m}^{-3}$ and 7.10×10^{15} molecules. cm^{-2} , respectively, which are lower or
20 equivalent to those documented in other urban areas. The seasonal and monthly variabilities of NH₃
21 concentrations in Paris are driven by sporadic agricultural emissions influenced by meteorological
22 conditions, with NH₃ concentrations in spring up to 2 times higher than in other seasons.

23 The potential source contribution function (PSCF) reveals that the close (100-200km) east and
24 northeast regions of Paris constitute the most important potential emission source areas of NH₃ in the
25 megacity.

26 Weekly cycles of NH₃ derived from satellite and ground-based observations show different ammonia
27 sources in Paris. In spring, agriculture has a major influence on ammonia concentrations and, in the
28 other seasons, multi-platform observations suggest that ammonia is also controlled by traffic-related
29 emissions.

30 In Paris, the diurnal cycle of NH₃ concentrations is very similar to the one of NO₂, with morning
31 enhancements coincident with intensified road traffic. NH₃ evening enhancements synchronous with
32 rush hours are also monitored in winter and fall. NH₃ concentrations measured during the weekends
33 are consistently lower than NH₃ concentrations measured during weekdays in summer and fall. This is
34 a further evidence of a significant traffic source of NH₃ in Paris.

35 1. Introduction

36 Ammonia (NH₃) is an air pollutant which plays a role in important environmental and health issues
37 [Rockström et al., 2009]. It is a highly reactive gas, with a lifetime of a few hours to a few days
38 [Evangelidou et al., 2021; Dammers et al., 2019], capable of reacting with nitrogen oxides (NO_x) and
39 sulfur oxides (SO_x) to form fine particulate matter composed of ammonium nitrate and ammonium
40 sulfate [Sutton et al., 2013]. The formation of fine particles plays a major role in the degradation of air
41 quality, as they are the cause of respiratory and cardiovascular diseases [Pope III et al., 2009].

42 Models have difficulty predicting events of particulate pollution associated with NH₃ since ground-
43 based atmospheric observations of this gas are still relatively sparse [Nair and Yu, 2020] and difficult
44 to implement [Twigg et al., 2022; von Bobruzki et al., 2010]. To our knowledge, only six countries in
45 the world (United States, China, the Netherlands, United Kingdom, Belgium, and Canada) have
46 dedicated NH₃ observations in their atmospheric monitoring networks. This poses a problem for long-
47 term monitoring of pollution and the implementation of emission reduction policies.

48 Global population growth causes increased food demand leading to higher ammonia emissions from
49 intensive agricultural production systems [Fowler et al., 2013]. Global NH₃ emissions have increased
50 by more than 80% between 1970 and 2017 [McDuffie et al., 2020]. In Europe, a substantial increase in
51 nitrate and ammonium concentrations in the composition of fine particles has been observed for several
52 years in the early spring when fertilizer applications intensify [Favez et al., 2021]. In addition, the share
53 of emissions related to road traffic is also increasing because of popularization of catalytic converters
54 in car engines [Zhang et al., 2021]. In France, 98% of ammonia comes from agricultural activities, via
55 decomposition and volatilization of nitrogen fertilizers (34%) and animal waste (64%), the rest are from
56 industry, road traffic and residential heating [CITEPA, 2022]. In the Ile-de-France region (Paris greater
57 area), the share of agriculture is lower (75%) due to a higher contribution of traffic and residential
58 sectors (13% and 12%, respectively [AirParif, 2022]). NH₃ emissions from road traffic are very poorly
59 quantified and may be a larger than expected source in urban areas [Pu et al., 2023; Chatain et al.,
60 2022; Cao et al., 2021; Roe et al., 2004; Sutton et al., 2000].

61 Monitoring NH₃ is therefore essential, especially in urban areas such as in Paris, where particulate
62 pollution episodes are observed almost every spring [Viatte et al., 2022] and often associated with
63 emissions from agricultural activities in the surrounding areas [Viatte et al., 2021; Kutzner et al., 2021;
64 Viatte et al., 2020; Petetin et al., 2016; Petit et al., 2015].

65 Global scale measurement of atmospheric ammonia is possible via soundings from several satellite-
66 borne instruments such as AIRS [Warner et al., 2016], CrIS [Shephard and Cady-Pereira, 2015], and IASI
67 [Clarisse et al., 2009]. Satellite measurements of atmospheric ammonia allow a description of its spatial
68 distribution with global coverage. The detection of the multi-year evolution of concentrations is
69 possible, as well as the detection of emission sources at the kilometer scale [Van Damme et al., 2018],
70 and even the quantification of their variability [Van Damme et al., 2021; Dammers et al., 2019]. Remote
71 sensing data are also used as a mean to estimate ammonia emission inventories [Marais et al., 2021;
72 Cao et al., 2020; Fortems-Cheiney et al., 2020].

73 Quantifying and analyzing temporal NH₃ variabilities at different scales (diurnal, weekly, seasonal, and
74 interannual) helps to improve emission inventories and air quality forecasts [Cao et al., 2021]. Diurnal
75 NH₃ variability, which is rarely measured, is particularly crucial because atmospheric models have
76 difficulty representing it [Lonsdale et al., 2017]. NH₃ concentrations increase during the day due to the

77 temperature dependence of emissions, but there may be many other factors at play influencing the
78 diurnal variability of NH₃ concentrations in the atmosphere, such as transport, boundary layer height,
79 deposition, fertilizer application time, road traffic emissions, and the interaction of all these factors
80 [Sudesh and Kulshrestha, 2021; Osada, 2020; Wang et al., 2015]. The diurnal variability of NH₃, which
81 is still largely missing from the ground and satellite observations, provides valuable information
82 regarding sources, surface exchange, deposition, gas-particle conversion, and transport of NH₃
83 [Clarisse et al., 2021].

84 In this work, we present 2.5-years of atmospheric NH₃ concentrations measured in Paris using the
85 synergy of ground-based and IASI satellite observations to quantify NH₃ variabilities at different time
86 scales.

87 **2. Methodology**

88 **2.1. miniDOAS**

89 NH₃ concentrations are measured since January 2020 in the Paris city-center (48.8°N, 2.3°E) using the
90 ground-based miniDOAS instrument located at the QUALAIR super-site (40 meters above ground level,
91 <https://qualair.fr/index.php/en/english/>). To the best of our knowledge this dataset constitutes the
92 only continuous (day and night) NH₃ observations available at high temporal frequency representative
93 of the Paris megacity. The miniDOAS (Differential Optical Absorption Spectroscopy) is a state-of-art
94 instrument suitable for NH₃ monitoring [Sintermann et al., 2016; Berkhout et al., 2017] since it
95 performs accurate high temporal resolution measurements (every hour, day and night) [Volten et al.,
96 2012]. It has been designed and developed by the National Institute for Public Health and the
97 Environment (RIVM, Netherlands) to be part of the Dutch National Air Quality Monitoring Network
98 [Berkhout et al., 2017]. The miniDOAS is an active remote sensing instrument based on open-path
99 differential absorption spectrometry. It uses a xenon lamp which emits a UV light, ammonia having a
100 strong absorption band in the UV between 200 and 230 nm. The UV light beam travels along an optical
101 path of 20 m, at the end of which there is a reflector which reflects the UV light and sends it back to
102 the spectrometer/receiver. The Beer-Lambert law is used to quantify the extinction at the absorption
103 wavelengths of ammonia to retrieve atmospheric ammonia concentrations [Volten et al., 2012]. The
104 miniDOAS can measure a wide range of ammonia concentrations (from 0.5 to 200 µg.m⁻³) day and
105 night and does not suffer from sampling artifacts, since it does not use a filter or inlet, unlike other
106 commonly used instruments (such as Picarro, [Caville et al., 2023; von Bobruzki et al., 2010]).
107 Estimated errors are 4.10⁻³ µg.m⁻³ on hourly measurements [Volten et al., 2012]. Using ammonia
108 measurements performed from this miniDOAS in Paris, Viatte et al. (2021) demonstrated the
109 contribution of NH₃ to particulate pollution events that occurred during the 2020 COVID lockdown.

110 **2.2. IASI**

111 The Infrared Atmospheric Sounding Interferometer (IASI, [Clerbaux et al., 2009]) was launched first in
112 2006 as part of the Metop satellite series to monitor atmospheric composition twice a day (at 9:30 and
113 21:30) globally. IASI measures atmospheric spectra in the thermal infrared region with an elliptical
114 pixel footprint of 12 × 12 km at nadir and 20 × 39 km at the far end of the swath. In this study, we use
115 NH₃ columns derived from IASI morning (9:30) overpasses onboard Metop B and C from January 2020
116 to June 2022. When comparing IASI and miniDOAS NH₃ concentrations in Paris, we have selected
117 coincident observations made within the same hour and the center of the IASI pixels was used to

118 determine the distance between the miniDOAS and IASI measurements. In this work, we use version
119 3 of the ANNI-NH₃ reanalyzed dataset [Van Damme et al., 2021; Guo et al., 2021; Viatte et al., 2022].

120 **2.3. Meteorological data from ERA-5**

121 Meteorological parameters originate from the ERA-5 database of the European Centre for Medium-
122 Range Weather Forecasts (ECMWF, [Hersbach et al., 2020]), which is built from observations
123 recalibrated into a global assimilation model at a 30 km resolution. In this work, we used the hourly
124 data of the temperature at 2 m, the precipitation, the u and v components of the wind at 100 m and
125 the height of the boundary layer, taken from the grid cells in which Paris is located.

126 **2.4. Back-trajectories and Potential Source Contribution Factor (PSCF) analysis**

127 To study the transport affecting concentration of ammonia in Paris, we use the Hybrid Single-Particle
128 Lagrangian Integrated Trajectory model (HYSPLIT, [Stein et al., 2015]) to calculate backward
129 trajectories of air masses ending at altitudes of 100 m (above sea level which corresponds to the
130 altitude of the miniDOAS location) between January 2020 and June 2022.

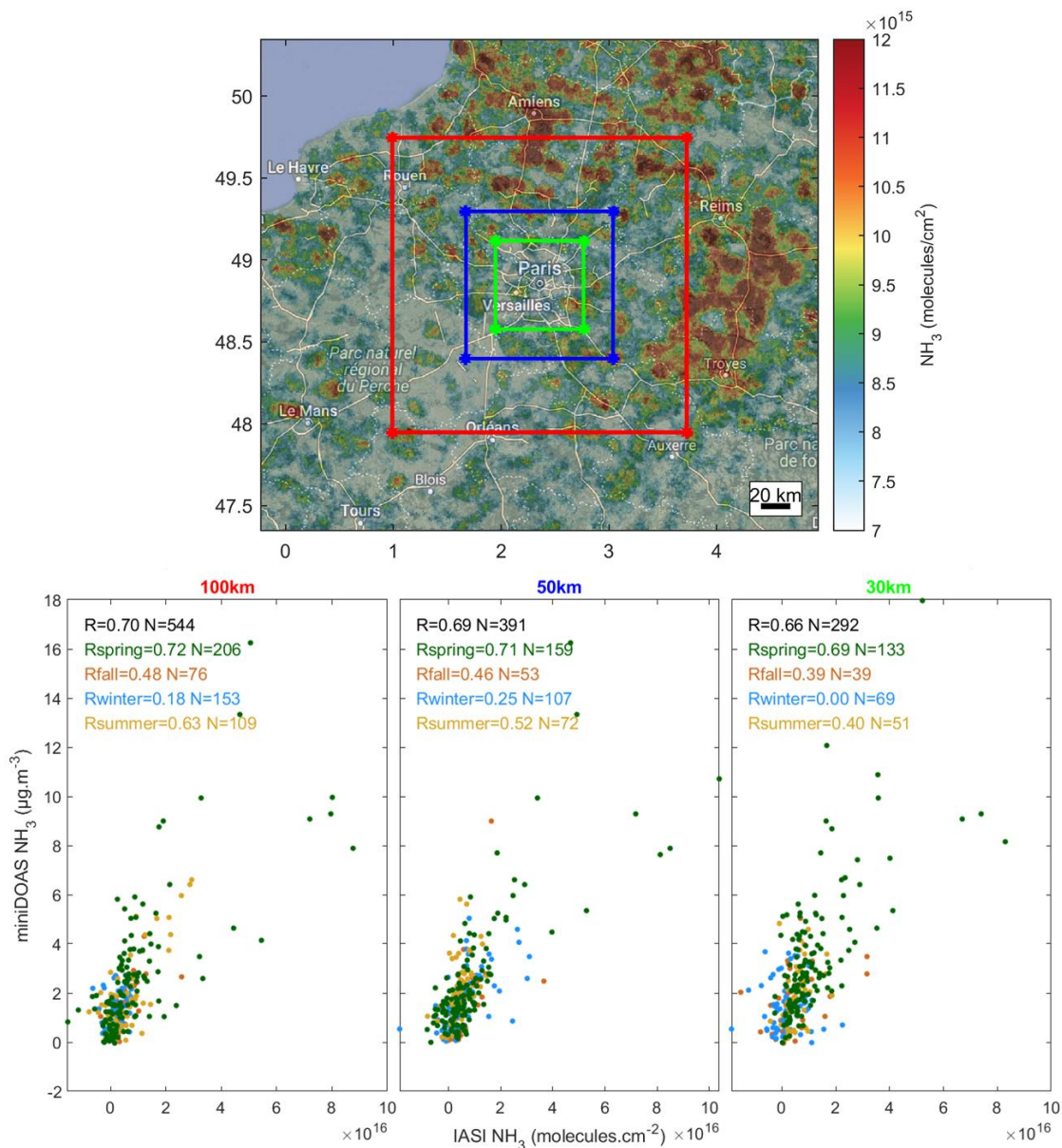
131 Meteorological data used in the runs are from the National Centers for Environmental Prediction
132 (NCEP) / National Center for Atmospheric Research (NCAR) reanalysis at 2.5-degree global latitude-
133 longitude projection. We ensure by visual inspections that the back trajectories using a 2.5° resolution
134 meteorological dataset are similar to using a finer meteorological dataset at 0.25° resolution (GFS).

135 Due to the short and highly variable lifetime of NH₃, ranging between 2-4 hours [Dammers et al., 2019]
136 and 12-hours [Evangelidou et al., 2021], we simulated an average 6-h backward trajectories with an
137 interval of one hour. Using the hourly NH₃ observations from the miniDOAS, the potential emission
138 sources of NH₃ were analyzed. The Potential Source Contribution Factor (PSCF) method [Malm et al.,
139 1986] is used to identify source regions affecting air quality in term of NH₃ concentration in Paris
140 between January 2020 and June 2022. This method is now commonly used in atmospheric science
141 [Wang et al., 2023; Qadri et al., 2022; Martino et al., 2022; Biuki et al., 2022; Ren et al., 2021; Zachary
142 et al., 2018; Jeong et al., 2011] and combines the concentration dataset with air parcel back-trajectory
143 to identify preferred pathways producing high observed NH₃ concentrations in Paris. The larger PSCF
144 (range: 0–1), the greater contribution of the pollution region to the atmospheric pollutants at the
145 receptor site.

146 **3. Results**

147 **3.1. Comparison of NH₃ concentrations between IASI and mini-DOAS**

148 The 2.5-years mean NH₃ total column distribution around Paris derived from IASI from January 1st 2020
 149 to May 31st 2022 is shown in Figure 1 (top panel). To obtain averages at a high resolution needed for
 150 Greater Paris-scale studies, we used the oversampling method described by van Damme et al. (2018)
 151 that takes into account the real elliptical sizes of each IASI pixel. All IASI maps shown in this study were
 152 computed using this methodology. Hot spots of ammonia are found around Paris in agricultural areas,
 153 especially in the Champagne-Ardennes region between Troyes and Reims cities [Viatte et al., 2020].



154
 155 *Figure 1: Top panel: 2.5-years average of IASI NH₃ column distributions (from January 1st 2020 to May*
 156 *31st 2022). Bottom panel: miniDOAS ground-based NH₃ concentrations (μg.m⁻³) versus IASI-retrieved*
 157 *NH₃ column concentrations (molecules.cm⁻²) per season for different spatial criteria from Paris city*
 158 *center where the miniDOAS is located (100km in red box, 50km in blue box, and 30km green box).*

159 NH₃ has a short atmospheric lifetime which is why we only compare miniDOAS data recorded within
160 the same hour as the IASI morning overpass time. The IASI-retrieved column (in molecules.cm⁻²) and
161 the miniDOAS ground-based concentrations (μg.m⁻³) are compared to assess the spatial criteria
162 (100km in red box, 50km in blue box, and 30km green box) and the season for which both datasets are
163 in best agreement. In this study we are not converting IASI columns to surface observations since it
164 introduces additional errors and does not change the correlation as explained in [Van Damme et al.,
165 2015].

166 Overall, the miniDOAS and IASI NH₃ concentrations are in moderate agreement with Pearson
167 correlation [Akoglu et al., 2018] of 0.70, 0.69, and 0.66 when considering IASI pixels within a 100km,
168 50km, and 30km box around Paris, respectively. The number of pairs is, however, reduced by a factor
169 of two when considering IASI pixels in a 100km versus a 30km box around Paris. All correlations are
170 significant (p-value < 0.05) except in winter for the 100km and 30km boxes, and in fall for the 30km
171 box. The best agreement between the miniDOAS and IASI is in spring, with Pearson correlations ranging
172 from 0.72 to 0.69 (green points in scatter plots of Figure 1). This period corresponds to high
173 atmospheric NH₃ concentrations when spreading practices occur in the surrounding agricultural
174 regions of Paris [Viatte et al., 2022]. The high correlation in spring between the two datasets can be
175 attributed to two factors: 1) NH₃ concentrations are higher and therefore the signal measured by the
176 two instruments are larger leading to a better correlation from the wide range of NH₃ concentrations
177 (0-18 μg.m⁻³ for the miniDOAS and 0-1.10¹⁶ molecules.cm⁻² for IASI, Figure 1) and 2) the high amount
178 of NH₃ emitted in spring in the surrounding regions due to fertilizer applications can be transported to
179 Paris [Viatte et al., 2022; Viatte et al., 2021] resulting in high correlations between the ~12-km IASI
180 footprints and the local miniDOAS observations. In fall and summer, the Pearson correlation
181 coefficients range from 0.63 to 0.40 between IASI and the miniDOAS for all boxes sizes. The lower
182 correlations between the ground-based and the satellite NH₃ observations could reveal specific NH₃
183 sources in the close vicinity of the miniDOAS which might be not representative of the IASI pixels size. In
184 winter, the agreements are poor between the miniDOAS and IASI because NH₃ concentrations are
185 weak and IASI is less sensitive to lower atmospheric layers when thermal contrast is low [Van Damme
186 et al., 2014].

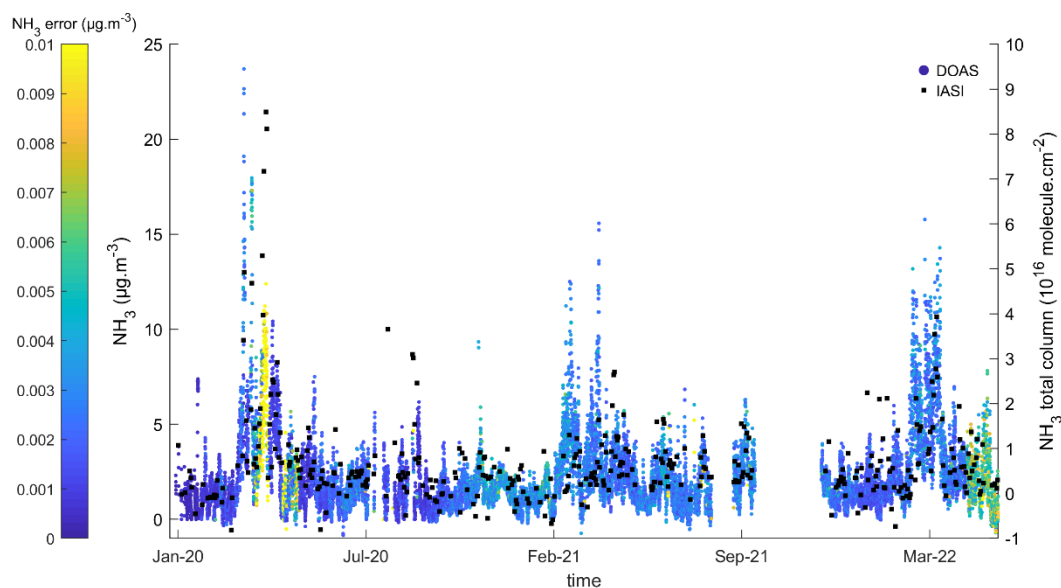
187 A trade-off between good correlations and keeping a sufficient number of collocations is found when
188 comparing NH₃ concentrations from ground-based measurements located in the Paris city-center with
189 the IASI dataset in a 50 km box. We chose for the rest of the analysis IASI dataset within the 50 km box
190 to analyze temporal variabilities of NH₃ in Paris.

191 **3.2. Impact of agriculture on NH₃ concentrations in Paris**

192 **3.2.1 2.5-years of NH₃ measurements in Paris**

193 Here, we investigate temporal variabilities of NH₃ using 2.5-years of hourly measurements from
194 January 1st 2020 to May 31st 2022 (Figure 2). The miniDOAS was working almost full time during this
195 period with 16 888 hourly measurements, out of the 21 145 possible. The missing data is due either to
196 some technical issues during warm conditions (malfunctioning aircondition in August 2021) or due to
197 its removal from the QUALAIR facility for field measurement campaigns (from September 15th 2021 to
198 November 24th 2021). Over the 16 888 hourly NH₃ measurements, average errors are 2.8 10⁻³ μg.m⁻³
199 with maximum values occurring when signal is low due to a transient poor alignment (such as in April

200 2020, yellow dots in Figure 2). Description of the measurement uncertainties can be found in Volten
201 et al. (2012).



202
203 *Figure 2: Timeseries of hourly NH₃ concentrations (in µg.m⁻³) color coded by the errors on*
204 *measurements derived from the miniDOAS located in Paris, and IASI NH₃ total columns (in black,*
205 *molecule.cm⁻²) observed in a 50km box centered in Paris from January 1st 2020 to May 31st 2022.*

206 The measurements made by the miniDOAS over the period January 2020 - June 2022 (N=16 888) show
207 an average ammonia concentration of 2.23 µg.m⁻³ in Paris over this period, with a standard deviation
208 of 2.02 µg.m⁻³, indicating a high NH₃ variability. In comparison, the average concentration measured
209 by the miniDOAS in an agricultural site at Grignon [Loubet et al., 2022] in September-October 2021
210 (France) is 6.52 ± 8.44 µg.m⁻³ [Claville et al., 2023], almost three times higher than in Paris. The
211 relatively low concentrations observed in Paris are explained by the distance to the major emission
212 sources which are related to agricultural activities. Ammonia concentrations measured in Paris are on
213 average lower or equivalent to those documented in urban areas such as Beijing (China, average of 21
214 ± standard deviation of 14 ppb corresponding to 14.7 ± 10 µg.m⁻³ from January 2018 to January 2019,
215 [Lan et al., 2021]), Shanghai (China, 6.2 ± 4.6 ppb which corresponds to 4.3 ± 3.2 µg.m⁻³ from July 2013
216 to September 2014, [Wang et al., 2015]), Rome (Italy, 1.2–21.6 µg.m⁻³ between May 2001 and March
217 2002, [Perrino et al., 2002]), Milan (Italy, 4.4–13.4 µg.m⁻³ between 2007 and 2019, [Lonati et al., 2020]),
218 Louisville (Unites-States, 2.2–5.2 µg.m⁻³ from June to August 2011, [Li et al., 2017]) and Toronto
219 (Canada, 2.5 ppb which corresponds to 1.75 µg.m⁻³ from 2003 to 2011, [Hu et al. 2014]). The miniDOAS
220 is located at an altitude of 40m so that its observation footprint is representative of the Greater Paris.
221 This may partly explain the lower NH₃ concentrations observed in Paris compared to other urban areas.

222 The miniDOAS and IASI coincident measurements show relatively low interannual variability (Table 1).
223 NH₃ annual concentrations measured by the miniDOAS are 2.06 ± 2.09 µg.m⁻³ and 2.04 ± 1.56 µg.m⁻³
224 for 2020 and 2021, respectively. The higher mean and standard deviation in 2022 (2.91 ± 2.40 µg.m⁻³
225 for the miniDOAS) compared to the other years can be due the fact that measurements are performed
226 from January to June only. IASI NH₃ total columns around Paris exhibit a higher NH₃ annual
227 concentration and standard deviation in 2020 compared to the other years because of the multiple

228 high pollution events occurring in spring during the 2020-COVID lockdown as described in Viatte et al.
 229 (2021).

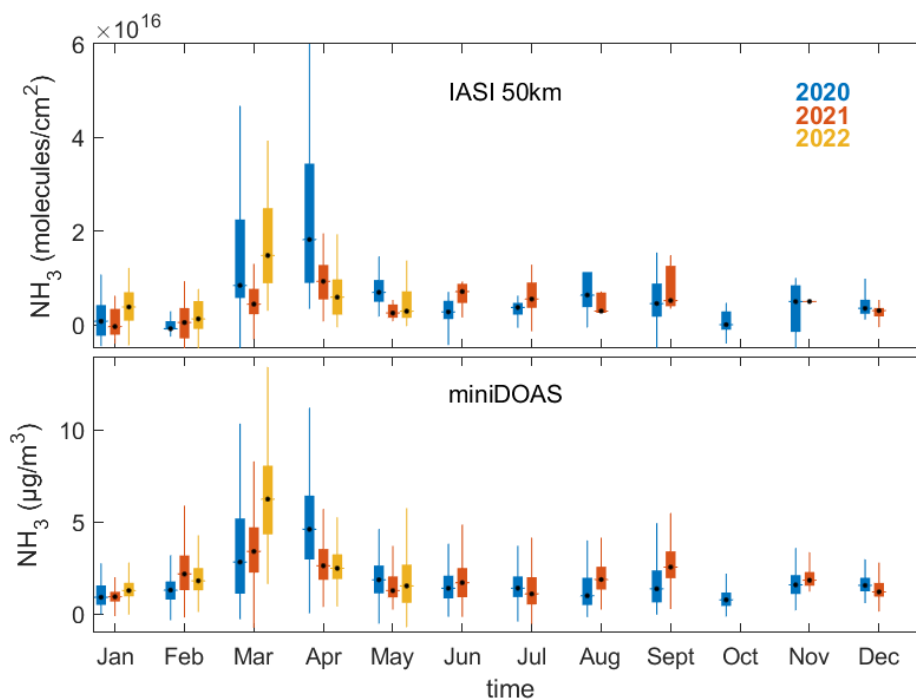
230 *Table 1: Average NH₃ concentration, standard deviation, and number of observations for 2020, 2021*
 231 *and part of 2022 derived from coincident measurements of the miniDOAS and IASI (50 km box around*
 232 *Paris).*

years	2020		2021		2022	
	miniDOAS	IASI (50km)	miniDOAS	IASI (50km)	miniDOAS	IASI (50km)
NH ₃ concentration (μg.m ⁻³ or molecules.cm ⁻²)	2.06	8.60 10 ¹⁵	2.04	5.48 10 ¹⁵	2.91	6.76 10 ¹⁵
Standard deviation (μg.m ⁻³ or molecules.cm ⁻²)	2.09	1.58 10 ¹⁶	1.56	5.69 10 ¹⁵	2.40	9.35 10 ¹⁵
Number of observations	7164	166	6182	134	3542	91

233

234 3.2.2 Seasonal and monthly NH₃ variabilities in Paris

235 Unlike the weak interannual variability of NH₃ concentrations in Paris, both ground-based (miniDOAS)
 236 and satellite (IASI) measurements reveal high seasonal variabilities of NH₃ concentrations (Figure 3). In
 237 spring, NH₃ concentration measured in Paris by the miniDOAS and IASI are on average
 238 $3.34 \pm 2.67 \mu\text{g.m}^{-3}$ and $1.21 \times 10^{16} \pm 1.57 \times 10^{16}$ molecules.cm⁻², respectively. These springtime NH₃
 239 concentrations are enhanced by a factor of two compared to the other seasons, which is consistent
 240 with the fertilizer application periods over the nearby agricultural fields. Both datasets show that NH₃
 241 concentrations in March and April are 2 to 3 times higher than the other months. Precipitation for
 242 these months is also lower than in February on average (see supplementary Figure S1).



243

244 *Figure 3: Monthly NH₃ concentrations color coded by the year of measurements (2020 in blue, 2021 in*
 245 *orange, and 2022 in yellow) derived from IASI (top panel, in molecules.cm⁻²) in a 50km box around Paris*

246 *and the ground-based miniDOAS instrument (bottom panel, in $\mu\text{g.m}^{-3}$) located in Paris city-center. Note*
247 *that IASI observations are only considered when a miniDOAS observation is available within the same*
248 *hour than IASI overpass.*

249 When considering each year of measurement separately, we notice that the timing of the maximum
250 NH_3 concentrations is variable. In 2020, the maximum is reached in April with averaged NH_3
251 concentrations of $4.76 \pm 2.48 \mu\text{g.m}^{-3}$ (miniDOAS) and $2.90 \times 10^{16} \pm 2.85 \times 10^{16}$ molecules. cm^{-2} (IASI),
252 whereas in 2022 the maximum appears in March with a monthly NH_3 concentration of 6.42 ± 2.46
253 $\mu\text{g.m}^{-3}$ and $1.72 \times 10^{16} \pm 1.04 \times 10^{16}$ molecules. cm^{-2} derived from the miniDOAS and IASI, respectively.

254 Meteorological conditions influence the timing of the agricultural practices (farmers do not spread
255 their fertilizer when it rains), NH_3 volatilization from the soil to the atmosphere (higher temperature
256 favors NH_3 volatilization [Sutton et al., 2013]), and the transport of NH_3 over Paris.

257 In April 2020, NH_3 concentrations observed by IASI and the miniDOAS are high compared to April 2022.
258 In April 2020, precipitation is low (0.3 mm compared to 0.75mm in April 2022) and the monthly
259 averaged atmospheric temperature is on 3 to 5°C higher than in 2021 and 2022 (Figure S1). This could
260 explain why NH_3 concentrations are higher in April 2020 than in 2022. Similarly, the lower ammonia
261 concentration recorded in March 2021 compared to March 2022 is likely explained by higher
262 precipitation (0.09 mm) and a lower temperature (of 2°C on monthly average) than in March 2022.

263 In 2021, a second NH_3 enhancement is measured in September by the miniDOAS ($2.73 \pm 1.14 \mu\text{g.m}^{-3}$)
264 and IASI ($7.93 \times 10^{15} \pm 4.64 \times 10^{15}$ molecules. cm^{-2}) which is not observed in 2020 possibly because
265 atmospheric temperatures were lower than in 2021 (Figure S1). The pronounced seasonal variability
266 can be explained in the first order by the practices of the farmers. In most European countries, strict
267 regulations are applied in term of the timing of fertilizer application [Ge et al., 2020]. In France, it is
268 forbidden to spread nitrogen fertilizers in winter months (between November 30th and February 15th,
269 [Ludemann et al., 2022]) depending on fertilizer and land/crop types.

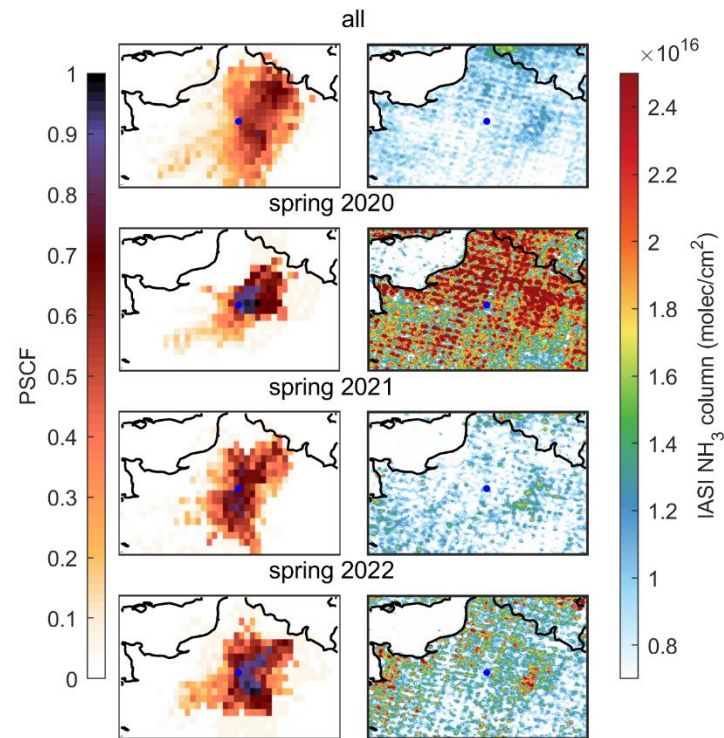
270 Overall, the seasonal and monthly variabilities of NH_3 concentrations in Paris are dominated by
271 agricultural activities and meteorological conditions.

272 **3.2.3 Potential Source Contribution Function (PSCF) analysis for NH_3 concentrations**

273 To determine the origin of the NH_3 measured in Paris, the Potential Source Contribution Function
274 (PSCF) is used. The PSCF analysis, as well as the IASI NH_3 maps, are shown for the investigated period
275 (January 2020 – June 2022, Figure 4 upper panels), and in the spring of 2020, 2021, and 2022 (Figure
276 4, three lower panels).

277 Over the whole timeseries, the northeast (100 km from Paris in the Aisne department of France) and
278 east (70km from Paris in the “Seine et Marne” department) locations are found to affect the NH_3
279 concentrations observed in the city between January 2020 and June 2022. These areas are indeed
280 source regions of NH_3 according to coincident IASI observations (Figure 4, upper panels). According to
281 wind fields parameters derived from ERA-5 over Paris (not shown here), the winds from the south are
282 more intense (up to 18 m.s^{-1}) and are related to lower ammonia concentrations (between 0 and $4 \mu\text{g.m}^{-3}$).
283 The northern winds are on average weaker (maximum around 12 m.s^{-1}) and are associated with
284 higher ammonia concentrations. In particular, for the northeast section the measured NH_3
285 concentration is found to exceed $8 \mu\text{g.m}^{-3}$.

286 According to the PSCF analysis, the main sources of NH₃ from agricultural activities are found in the
 287 close areas of Paris (within 100 and 200 km from Paris city-center) mainly from the east and northeast
 288 directions. In France, the averaged utilized agricultural area per department in 2020 is 64.5 ha (Agreste
 289 – Recensements agricoles, <https://stats.agriculture.gouv.fr/cartostat/#c=home>). The highlighted
 290 departments by the PSCF analysis are ranked to have the most cultivated areas in France with 141.5
 291 ha for Seine et Marne, 124.4 ha for Oise, and 110.4 ha for Aisne departments for instance.
 292



293 *Figure 4: Potential Source Contribution Function (PSCF, left) and IASI NH₃ total columns (right, in*
 294 *molecules.cm⁻²) The top row is the January 2020 to June 2022 average, and the 3 lower panels are for*
 295 *spring 2020, 2021, and 2022. The blue dot indicates the location of Paris.*
 296

297 In spring, when NH₃ concentrations are significantly higher in Paris (Figure 3) and in the surroundings
 298 (Figure 4 three lower right panels), the PSCF analysis show that the northeast and southeast regions
 299 are the major sources of the observed NH₃ concentrations in Paris. In spring 2020, NH₃ columns are
 300 higher than in spring 2021 and 2022, according to IASI observations. The main sources of NH₃ in spring
 301 2020 are pronounced in the nearby east-northeast areas (at 50 km from Paris in the surrounding
 302 departments of Seine et Marne, Oise, and Val d’Oise). In spring 2021, IASI observations reveal lower
 303 NH₃ columns than in 2020 and 2022 and the sources of NH₃ concentrations in Paris are in the
 304 surrounding regions of Paris (100 km in all directions). In spring 2022, the northeast pathway is
 305 highlighted similarly to spring 2020 but with a contribution of the southeast region as well.

306 **3.3 Effect of road traffic on NH₃ variability in Paris**

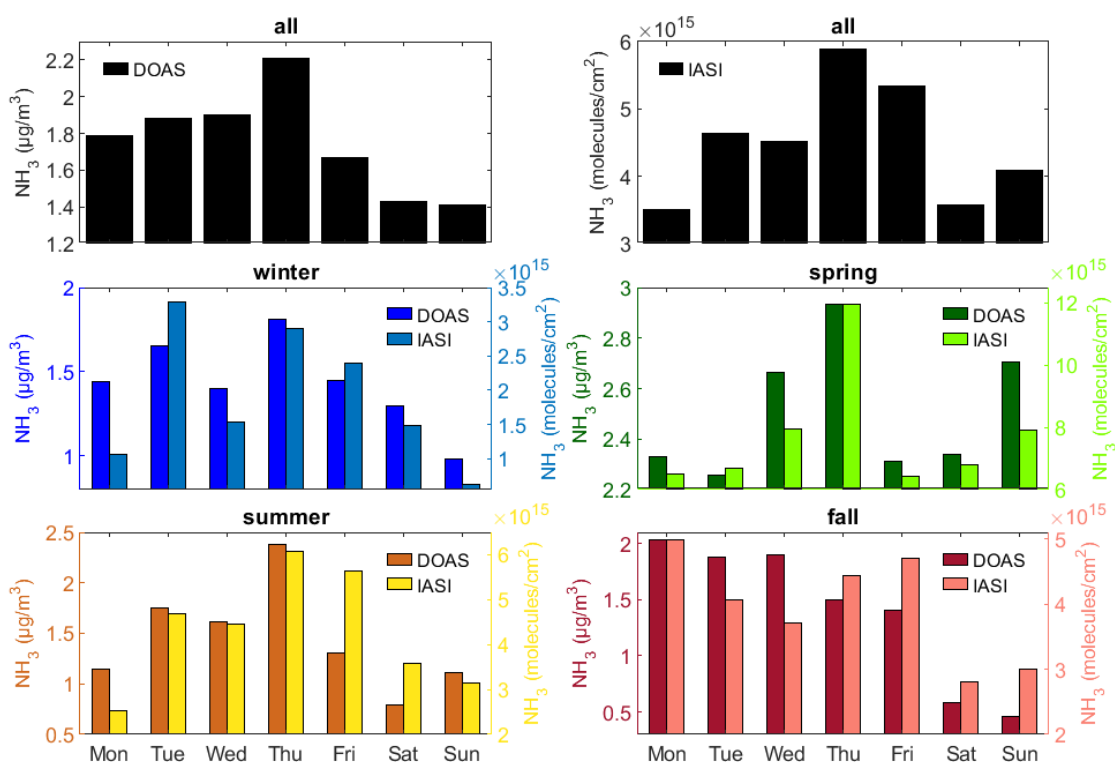
307 **3.3.1 Weekly cycle of NH₃ concentrations**

308 The weekly cycles of ammonia concentrations measured in Paris by the miniDOAS and IASI over the
309 studied timeseries are presented in Figure 5 (black bars, top panels). Both datasets show an increase
310 of ammonia concentrations during the week, reaching a maximum on Thursday (2.21 µg.m³ for the
311 miniDOAS and 5.90x10¹⁵ molecules.cm⁻² for IASI).

312 The weekly cycle of IASI measurements in Paris is almost analogous to the one observed over European
313 agricultural areas with low concentrations observed on Mondays, as a result of reduced NH₃ emissions
314 over the weekend, and an accumulation of ammonia during the week [Van Damme et al., 2022]. In
315 addition, the IASI NH₃ weekly cycle averaged over 2.5-years of measurements in Paris is very similar to
316 the NH₃ weekly cycle measured in spring (Figure 5) when agricultural activities intensify. Monitoring
317 similar NH₃ weekly variability in the urban area of Paris demonstrates that agricultural activities in the
318 surrounding areas control the variability of ammonia in Paris on average over the whole season.

319 The NH₃ weekly cycle observed over 2.5-years of measurements from the ground-based miniDOAS and
320 the IASI satellite observations show, however, relatively low NH₃ concentrations on Saturday and
321 Sunday. The cycle is less pronounced for IASI measurements. Ammonia concentrations observed over
322 the weekend by the miniDOAS and IASI are lower by 25% and 20% compared to NH₃ concentrations
323 averaged over the weekdays in Paris.

324 When considering intraweek variabilities by seasons (Figure 5, four lower panels), one can observe
325 that both IASI and the miniDOAS dataset reveal similar NH₃ weekly cycles. The NH₃ miniDOAS
326 measurements and coincident IASI total columns measured in a 50km box around Paris exhibit lower
327 concentrations over the weekends compared to weekdays for all seasons, except in spring for which
328 higher NH₃ concentrations are found on Wednesday and Sunday. In spring, the miniDOAS and IASI
329 measure a difference of NH₃ concentrations averaged over the weekends compared to weekdays of
330 +1% and -7%, respectively. In fall, summer, and winter, the miniDOAS (IASI) instrument measure a
331 decrease of NH₃ concentrations between weekends and weekdays of 70% (34%), 42% (28%), and 27%
332 (53%) respectively.



334

335 *Figure 5: Day of the week NH_3 concentrations derived from the miniDOAS ($\mu\text{g}\cdot\text{m}^{-3}$) and IASI*
 336 *($\text{molecules}\cdot\text{cm}^{-2}$) in Paris for the investigated period (January 2020 to May 2022, top panels), and for*
 337 *different seasons (winter in blue, spring in green, summer in brown and yellow, and fall in red and pink*
 338 *bars).*

339 Comparing these weekly variabilities with those of the weekly flow of cars in Paris (Figure S2), the same
 340 pattern is clearly highlighted with a stable number of cars per hour from Monday to Friday (around
 341 640) and a decrease of 14% over the weekends.

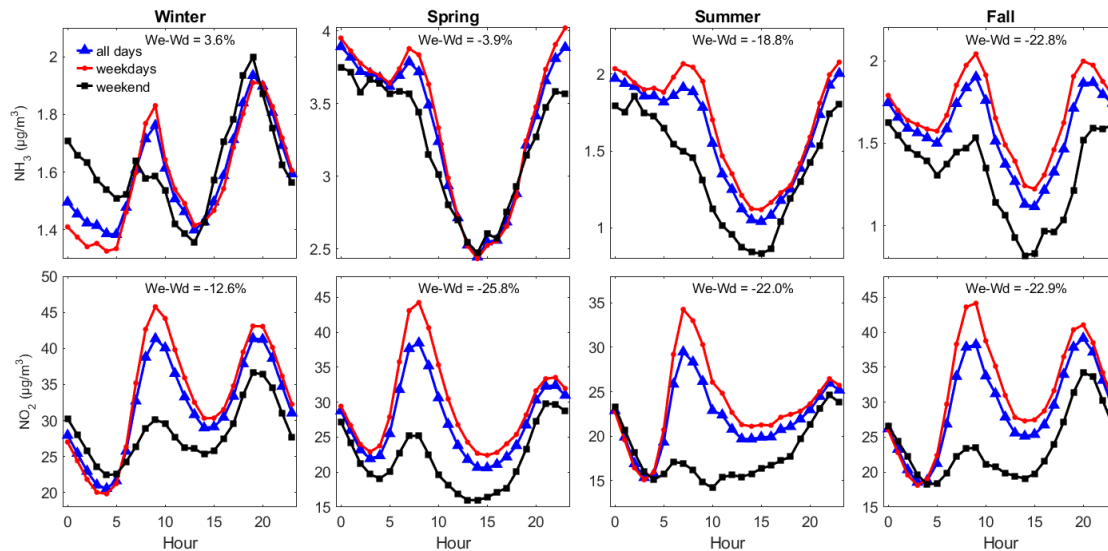
342 We can make the hypothesis that during all seasons except spring, the influence of the agricultural
 343 practices on the variability of ammonia in Paris is less pronounced, revealing NH_3 contribution from
 344 the traffic source. Since the road traffic intensity is constant throughout the year in Paris, the
 345 proportion of ammonia emitted from road traffic is proportionally higher outside the fertilization
 346 period.

347 3.3.2 Diurnal cycle of NH_3 concentration in Paris

348 With the high temporal resolution of the mini-DOAS acquisitions, the diurnal variability of NH_3
 349 concentration is assessed in Paris using, for the first time, a quasi-continuous (temporal coverage of
 350 80%) and a relatively long timeseries of 2.5-years of NH_3 observations.

351 Hourly NH_3 concentrations measured by the miniDOAS from January 2020 to May 2022 are shown in
 352 Figure S3. It shows a marked diurnal variability of NH_3 , with a decrease of about 30% in the middle of
 353 the day (around 14:00 LT) compared to the night, then an increase in the afternoon to reach again a
 354 maximum during the night.

355 Note that this diurnal variability of NH_3 measured by the miniDOAS is different than the one reported
 356 during springtime pollution episodes from a ground-based Fourier Transform InfraRed spectrometer
 357 located in the suburbs of Paris [Kutzner et al., 2021]. While measured integrated NH_3 total columns
 358 show an intraday increase until late afternoon, the miniDOAS measures NH_3 concentrations varying in
 359 opposition to the boundary layer height (Figure S3). This reflects the dynamical effect of the boundary
 360 layer height, which is controlled by atmospheric temperature, on the dilution of pollutants
 361 concentrations measured close to the surface. Such effect is also seen with surface measurements of
 362 NO_2 concentrations in Paris (Figure S3).



363
 364 *Figure 6: Diurnal variability of NH_3 (upper panels) and NO_2 (lower panels) concentrations measured by*
 365 *the miniDOAS and Airparif in ($\mu\text{g}\cdot\text{m}^{-3}$) averaged by seasons using 2.5-years of measurements in Paris.*
 366 *Hours are indicated in local time. The diurnal variability of NH_3 and NO_2 are shown in blue lines when*
 367 *considering all days, in red lines for weekdays, and in black lines for weekends.*

368 The diurnal variability of NH_3 concentrations presents an increase in the morning visible for all seasons
 369 (Figure 6). Between 5:00 and 8:00, road-traffic in Paris increases by a factor 4 (Figure S2) and NH_3
 370 concentrations rise by more than 20% in winter and fall, and about 3% in summer and spring.

371 To verify the hypothesis that road traffic is responsible for these morning enhancements, NO_2 diurnal
 372 variability is also shown in Figure 6 (lower panels). In Paris, NO_2 is considered as a proxy for road traffic
 373 emissions [Pazmino et al., 2022]. For all seasons, morning enhancements of NO_2 concentrations related
 374 to intensified road traffic emissions are coincident with morning enhancements of NH_3 concentrations.
 375 Similarly, enhancements of NO_2 and NH_3 concentrations are observed during the evenings (20:00 to
 376 22:00 LT) in winter and fall only. In spring, agriculture which is the overall dominant source of ammonia
 377 in Paris, prevents from monitoring NH_3 emitted from road traffic. Conversely, in fall and winter, the
 378 relative share of agriculture is weaker, and the peaks of NH_3 concentrations during rush hours (morning
 379 and evening) are clearly observed by the miniDOAS.

380 Diurnal variability of NH_3 and NO_2 concentrations averaged during weekdays (red lines) and weekends
 381 (black lines) are shown in Figure 6. NO_2 concentrations are systematically lower during weekends by
 382 12.6%, 25.8%, 22.0%, and 22.9% in winter, spring, summer, and fall respectively, compared to

383 weekdays. Similarly, diurnal cycle of NH₃ concentrations averaged during weekends are constantly
384 lower than NH₃ concentrations averaged during weekdays in summer and fall by 22.0% and 22.9%.

385 This highlights the importance of traffic emissions of NH₃ in such urban area of Paris, detected by
386 ground-based measurements when agricultural practices are reduced in the surrounding region.

387 These results are consistent with previous studies showing the importance of NH₃ emissions from
388 traffic in urban areas, such as in Rome (Italy, [Perrino et al., 2002]), in Beijing (China, [Ianniello et al.,
389 2010]), in Shanghai (China, [Wang et al., 2015]), and in Manchester (United Kingdom, [Whitehead et
390 al., 2004]) for instance. These emissions have gradually become another major contribution of
391 ammonia pollution in urban areas in the United States and China [Sun et al., 2017]. Ammonia emissions
392 from road vehicles are shown to be underestimated in the United Kingdom [Farren et al., 2020] and in
393 densely-populated areas in China [Wen et al., 2022]. In France, NH₃ levels measured at a traffic site of
394 Reims city are significantly higher than those observed in a background site [Chatain et al., 2022]. Our
395 results in Paris confirm that traffic has a significant contribution to atmospheric nitrogen budgets and
396 stress the need for further NH₃ monitoring in urban sites.

397 **4. Conclusion**

398 Temporal variabilities of NH₃ concentrations in Paris are assessed using joint observations of ground-
399 based (miniDOAS) and satellite (IASI) remote sensing observations from January 2020 to June 2022.
400 We present the first relatively long (2.5-years) and continuous record of hourly NH₃ concentrations in
401 Paris to determine temporal variabilities of ammonia at different scales (from interannual to diurnal
402 variability) to unravel emission sources (traffic and agriculture).

403
404 Qualitative comparison of NH₃ derived from the ground-based miniDOAS located in Paris city-center
405 and IASI satellite observations reveals an overall moderate agreement with Pearson's correlation
406 coefficients of 0.66, 0.69 and 0.70 when considering IASI observations in a 100km, 50km, and 30km
407 box around Paris. The best agreement between both datasets is found during springtime when NH₃
408 concentrations are 2 to 3 times higher than during the other seasons due to fertilizer spreading
409 occurring in the surrounding agricultural regions of Paris. Overall, agricultural activities driven by
410 favorable meteorological conditions (high temperature and low precipitation) control the seasonal and
411 monthly variabilities of NH₃ in Paris. The PSCF analyses indicate that the agricultural regions to the east
412 and northeast within 100 to 200 km from Paris city-center have the greatest impact on the NH₃ budget
413 in Paris.

414
415 Road-traffic emissions are noticeable in the weekly NH₃ cycles measured by satellite and ground-based
416 instruments, when agricultural related emissions are weak. Ammonia concentrations observed over
417 the weekend by the miniDOAS and IASI are lower by 25% and 20% compared to NH₃ concentrations
418 averaged over the weekdays. In addition, diurnal cycles of NH₃ concentrations in Paris are similar to
419 NO₂ and reveal coincident enhancements during rush hours. Further long-term NH₃ monitoring in
420 urban areas is needed to better estimate NH₃ emissions from the on-road sector and their impact on
421 secondary particle formation.

422
423 We have shown that the planetary boundary layer height greatly influences diurnal variabilities derived
424 from surface measurements. Future work will be carried to compare these NH₃ datasets in Paris to
425 atmospheric model outputs to evaluate the timing and the absolute value of emission inventories, as

426 well as the partition between NH₃ emission sectors (traffic vs. agriculture). The launch of the
427 geostationary MTG satellite carrying the hyperspectral sounder IRS, scheduled for 2024, will offer
428 unprecedented atmospheric observations with a spatial resolution of 4 km × 4 km (at the Equator) and a
429 high temporal resolution (every 30 minutes over Europe). These new observations will improve our
430 understanding of the diurnal variability of ammonia, and it will be a great addition to the miniDOAS
431 and IASI observations.

432

433 **Data availability**

434 The IASI NH₃ dataset used in this study are available via the Zenodo repository
435 <https://doi.org/10.5281/zenodo.7962362> (Viatte, 2023). The miniDOAS data are available here
436 https://iasi-ft.eu/products/nh3_minidoas/ (Viatte, 2023). The ERA-5 data are available via the Climate
437 Data Record (CDR) Copernicus website
438 <https://cds.climate.copernicus.eu/cdsapp#!/search?text=ERA5%20back%20extension&type=dataset>
439 (C3S CDS, 2023). The potential source contribution function is available via the Meteothink.org
440 <http://meteothink.org/docs/trajstat/pscf.html> (Wang et al., 2009). Last access to all URLs: 23 May
441 2023.

442

443 **Author contributions**

444 CV and NG designed the project. MVD and LC provided the IASI data. AH, AW, DS helped with the
445 miniDOAS installation and data acquisition. CV and CD analyzed the data. CV and CD wrote the
446 manuscript draft. All the co-authors reviewed and edited the manuscript. CC wrote proposals to
447 financially support the miniDOAS.

448 **Competing interests**

449 The authors declare that they have no conflict of interest.

450 **Acknowledgments**

451 IASI is a joint mission of EUMETSAT and the Centre National d'Etudes Spatiales (CNES, France). The IASI
452 Level 1C data are distributed in near real time by EUMETSAT through the EUMETCast system
453 distribution. The authors acknowledge the AERIS data infrastructure (<https://www.aeris-data.fr>) for
454 providing access to the IASI Level 1 radiance and Level 2 NH₃ concentration data used in this study.
455 CNES and the AC-SAF (CDOP3) project provided financial support for the miniDOAS acquisition. We
456 thank the NOAA's Air Resources Laboratory (ARL) for providing the HYSPLIT model. Research at ULB
457 was supported by the Belgian State Federal Office for Scientific, Technical and Cultural Affairs (Prodex
458 HIRS) and the Air Liquide Foundation (TAPIR project). LC is Research Associate supported by the Belgian
459 F.R.S.-FNRS. MVD is supported by the FED-tWIN project ARENBERG funded via the Belgian Science
460 Policy Office (BELSPO).

461

462 **References**

- 463 AERIS: NH₃ total column from IASI (Level 2), <https://iasi.aeris-data.fr/NH3/>, last access: 11 May 2023.
- 464 Airparif, 2022 : <https://www.airparif.asso.fr/surveiller-la-pollution/les-emissions>, last access 24 Feb
465 2023.
- 466 Akoglu, H.: User's guide to correlation coefficients, *Turkish J. Emerg. Med.*, 18(3), 91–93,
467 doi:<https://doi.org/10.1016/j.tjem.2018.08.001>, 2018.
- 468 Berkhout, A. J. C., Swart, D. P. J., Volten, H., Gast, L. F. L., Haaima, M., Verboom, H., Stefess, G.,
469 Hafkenscheid, T., and Hoogerbrugge, R.: Replacing the AMOR with the miniDOAS in the ammonia
470 monitoring network in the Netherlands, *Atmos. Meas. Tech.*, 10, 4099–4120,
471 <https://doi.org/10.5194/amt-10-4099-2017>, 2017.
- 472 Biuki, Z. A., Parvin, P. and Aghaei, M.: Satellite remote sensing of particulate matter in the atmosphere
473 of megacities: A case study of Tehran, Iran, *Atmos. Pollut. Res.*, 13(10), 101545,
474 doi:<https://doi.org/10.1016/j.apr.2022.101545>, 2022.
- 475 Cao, H., Henze, D. K., Cady-Pereira, K., McDonald, B. C., Harkins, C., Sun, K., Bowman, K. W., Fu, T.-M.
476 and Nawaz, M. O.: COVID-19 Lockdowns Afford the First Satellite-Based Confirmation That Vehicles
477 Are an Under-recognized Source of Urban NH₃ Pollution in Los Angeles, *Environ. Sci. Technol. Lett.*,
478 doi:10.1021/acs.estlett.1c00730, 2021.
- 479 Cao, H., Henze, D. K., Shephard, M. W., Dammers, E., Cady-Pereira, K., Alvarado, M., Lonsdale, C., Luo,
480 G., Yu, F., Zhu, L., Danielson, C. G. and Edgerton, E. S.: Inverse modeling of NH₃ sources using CrIS
481 remote sensing measurements, *Environ. Res. Lett.*, 15(10), 104082, doi:10.1088/1748-9326/abb5cc,
482 2020.
- 483 Caville et al.: Measurements of ammonia in ambient air and over a controlled artificial source during
484 the AMICA field campaign at a rural site in the Ile-de-France region, *Sensors*, to be submitted, 2023.
- 485 Chatain, M., Chretien, E., Crunaire, S. and Jantzem, E.: Road Traffic and Its Influence on Urban Ammonia
486 Concentrations (France), *Atmosphere (Basel)*, 13(7), doi:10.3390/atmos13071032, 2022.
- 487 CITEPA, 2022: [https://www.citepa.org/wp-content/uploads/publications/cee-
488 nu/UNECE_France_mars2022.pdf](https://www.citepa.org/wp-content/uploads/publications/cee-nu/UNECE_France_mars2022.pdf), last access 24 Feb 2023.
- 489 Clarisse, L., Van Damme, M., Hurtmans, D., Franco, B., Clerbaux, C., & Coheur, P.-F.: The diel cycle of
490 NH₃ observed from the FY-4A Geostationary Interferometric Infrared Sounder (GIIRS). *Geophysical
491 Research Letters*, 48, e2021GL093010, <https://doi.org/10.1029/2021GL093010>, 2021.
- 492 Clarisse, L., Clerbaux, C., Dentener, F., Hurtmans, D., and Coheur, P.-F.: Global ammonia distribution
493 derived from infrared satellite observations, *Nat. Geosci.*, 2, 479–483,
494 <https://doi.org/10.1038/ngeo551>, 2009.
- 495 Clerbaux, C., Boynard, A., Clarisse, L., George, M., Hadji-Lazaro, J., Herbin, H., Hurtmans, D., Pommier,
496 M., Razavi, A., Turquety, S., Wespes, C. and Coheur, P.-F.: Monitoring of atmospheric composition using
497 the thermal infrared IASI/MetOp sounder, *Atmos. Chem. Phys.*, 9(16), 6041–6054, doi:10.5194/acp-9-
498 6041-2009, 2009.

499 Copernicus Climate Change Service, Climate Data Store, (2023): ERA5 hourly data on single levels from
500 1940 to present. Copernicus Climate Change Service (C3S) Climate Data Store (CDS), DOI:
501 10.24381/cds.adbb2d47 (Accessed on 11-May-2023)

502 Dammers, E., McLinden, C. A., Griffin, D., Shephard, M. W., Van Der Graaf, S., Lutsch, E., Schaap, M.,
503 Gainairu-Matz, Y., Fioletov, V., Van Damme, M., Whitburn, S., Clarisse, L., Cady-Pereira, K., Clerbaux,
504 C., Coheur, P. F., and Erisman, J. W.: NH₃ emissions from large point sources derived from CrIS and IASI
505 satellite observations, *Atmos. Chem. Phys.*, 19, 12261–12293, [https://doi.org/10.5194/acp-19-12261-](https://doi.org/10.5194/acp-19-12261-2019)
506 2019, 2019.

507 Evangeliou, N., Balkanski, Y., Eckhardt, S., Cozic, A., Van Damme, M., Coheur, P.-F., Clarisse, L.,
508 Shephard, M. W., Cady-Pereira, K. E. and Hauglustaine, D.: 10-year satellite-constrained fluxes of
509 ammonia improve performance of chemistry transport models, *Atmos. Chem. Phys.*, 21(6), 4431–
510 4451, doi:10.5194/acp-21-4431-2021, 2021.

511 Farren, N. J., Davison, J., Rose, R. A., Wagner, R. L. and Carslaw, D. C.: Underestimated Ammonia
512 Emissions from Road Vehicles, *Environ. Sci. Technol.*, 54(24), 15689–15697,
513 doi:10.1021/acs.est.0c05839, 2020.

514 Favez, O., Weber, S., Petit, J.-E., Alleman, L. Y., Albinet, A., Riffault, V., Chazeau, B., Amodeo, T.,
515 Salameh, D., Zhang, Y., Srivastava, D., Samaké, A., Aujay-Plouzeau, R., Papin, A., Bonnaire, N.,
516 Boullanger, C., Chatain, M., Chevrier, F., Detournay, A., Leoz-Garziandia, E. (2021). Overview of the
517 French Operational Network for In Situ Observation of PM Chemical Composition and Sources in Urban
518 Environments (CARA Program), *Atmosphere*, 12(2), <https://doi.org/10.3390/atmos12020207>, 2021.

519 Fortems-Cheiney, A., Dufour, G., Dufossé, K., Couvidat, F., Gilliot, J.-M., Siour, G., Beekmann, M., Foret,
520 G., Meleux, F., Clarisse, L., Coheur, P.-F., Van Damme, M., Clerbaux, C., and Générumont, S.: Do
521 alternative inventories converge on the spatiotemporal representation of spring ammonia emissions
522 in France?, *Atmos. Chem. Phys.*, 20, 13481–13495, <https://doi.org/10.5194/acp-20-13481-2020>, 2020.

523 Fowler, D., et al.: The global nitrogen cycle in the twenty-first century, *Philos. Trans. R. Soc. B*,
524 368(1621), 1–13, doi:10.1098/rstb.2013.0164, 2013.

525 Ge, X., Schaap, M., Kranenburg, R., Segers, A., Reinds, G. J., Kros, H. and de Vries, W.: Modeling
526 atmospheric ammonia using agricultural emissions with improved spatial variability and temporal
527 dynamics, *Atmos. Chem. Phys.*, 20(24), 16055–16087, doi:10.5194/acp-20-16055-2020, 2020.

528 Guo, X., Wang, R., Pan, D., Zondlo, M. A., Clarisse, L., Van Damme, M., Whitburn, S., Coheur, P.-F.,
529 Clerbaux, C., Franco, B., Golston, L. M., Wendt, L., Sun, K., Tao, L., Miller, D., Mikoviny, T., Müller, M.,
530 Wisthaler, A., Tevlin, A. G., Murphy, J. G., Nowak, J. B., Roscioli, J. R., Volkamer, R., Kille, N., Neuman,
531 J. A., Eilerman, S. J., Crawford, J. H., Yacovitch, T. I., Barrick, J. D. and Scarino, A. J.: Validation of IASI
532 Satellite Ammonia Observations at the Pixel Scale Using In Situ Vertical Profiles, *J. Geophys. Res.*
533 *Atmos.*, 126(9), e2020JD033475, doi:<https://doi.org/10.1029/2020JD033475>, 2021.

534 Hersbach, H.; Bell, B.; Berrisford, P.; Hirahara, S.; Horányi, A.; Muñoz-Sabater, J.; Nicolas, J.; Peubey,
535 C.; Radu, R.; Schepers, D.; et al. The ERA5 global reanalysis. *Q. J. R. Meteorol. Soc.* 146, 1999–2049,
536 doi:10.1002/qj.3803, <https://www.ecmwf.int/en/forecasts/datasets/reanalysis-datasets/era5>, 2020.

537 Hu, Q., Zhang, L., Evans, G. J. and Yao, X.: Variability of atmospheric ammonia related to potential
538 emission sources in downtown Toronto, Canada, *Atmos. Environ.*, 99, 365–373,
539 doi:<https://doi.org/10.1016/j.atmosenv.2014.10.006>, 2014.

540 Ianniello, A., Spataro, F., Esposito, G., Allegrini, I., Rantica, E., Ancora, M. P., Hu, M. and Zhu, T.:
541 Occurrence of gas phase ammonia in the area of Beijing (China), *Atmos. Chem. Phys.*, 10(19), 9487–
542 9503, doi:[10.5194/acp-10-9487-2010](https://doi.org/10.5194/acp-10-9487-2010), 2010.

543 Jeong, U., Kim, J., Lee, H., Jung, J., Kim, Y. J., Song, C. H. and Koo, J.-H.: Estimation of the contributions
544 of long range transported aerosol in East Asia to carbonaceous aerosol and PM concentrations in
545 Seoul, Korea using highly time resolved measurements: a PSCF model approach, *J. Environ. Monit.*,
546 13(7), 1905–1918, doi:[10.1039/C0EM00659A](https://doi.org/10.1039/C0EM00659A), 2011.

547 Kutzner, R. D., Cuesta, J., Chelin, P., Petit, J.-E., Ray, M., Landsheere, X., Tournadre, B., Dupont, J.-C.,
548 Rosso, A., Hase, F., Orphal, J., and Beekmann, M.: Diurnal evolution of total column and surface
549 atmospheric ammonia in the megacity of Paris, France, during an intense springtime pollution episode,
550 *Atmos. Chem. Phys.*, 21, 12091–12111, <https://doi.org/10.5194/acp-21-12091-2021>, 2021.

551 Lan, Z., Lin, W., Pu, W. and Ma, Z.: Measurement report: Exploring NH₃ behavior in urban and suburban
552 Beijing: comparison and implications, *Atmos. Chem. Phys.*, 21(6), 4561–4573, doi:[10.5194/acp-21-4561-2021](https://doi.org/10.5194/acp-21-4561-2021), 2021.

554 Li, Y., Thompson, T. M., Van Damme, M., Chen, X., Benedict, K. B., Shao, Y., Day, D., Boris, A., Sullivan,
555 A. P., Ham, J., Whitburn, S., Clarisse, L., Coheur, P.-F. and Collett Jr., J. L.: Temporal and spatial variability
556 of ammonia in urban and agricultural regions of northern Colorado, United States, *Atmos. Chem. Phys.*,
557 17(10), 6197–6213, doi:[10.5194/acp-17-6197-2017](https://doi.org/10.5194/acp-17-6197-2017), 2017.

558 Lonati, G. and Cernuschi, S.: Temporal and spatial variability of atmospheric ammonia in the Lombardy
559 region (Northern Italy), *Atmos. Pollut. Res.*, 11(12), 2154–2163,
560 doi:<https://doi.org/10.1016/j.apr.2020.06.004>, 2020.

561 Lonsdale, C. R., Hegarty, J. D., Cady-Pereira, K. E., Alvarado, M. J., Henze, D. K., Turner, M. D., Capps, S.
562 L., Nowak, J. B., Neuman, J. A., Middlebrook, A. M., Bahreini, R., Murphy, J. G., Markovic, M. Z.,
563 VandenBoer, T. C., Russell, L. M., and Scarino, A. J.: Modeling the diurnal variability of agricultural
564 ammonia in Bakersfield, California, during the CalNex campaign, *Atmos. Chem. Phys.*, 17, 2721–2739,
565 <https://doi.org/10.5194/acp-17-2721-2017>, 2017.

566 Loubet, B., Buysse, P., Gonzaga-Gomez, L., Lafouge, F., Ciuraru, R., Decuq, C., Kammer, J., Bsaibes, S.,
567 Boissard, C., Durand, B., Gueudet, J.-C., Fanucci, O., Zurfluh, O., Abis, L., Zannoni, N., Truong, F.,
568 Baisnée, D., Sarda-Estève, R., Staudt, M. and Gros, V.: Volatile organic compound fluxes over a winter
569 wheat field by PTR-Qi-TOF-MS and eddy covariance, *Atmos. Chem. Phys.*, 22(4), 2817–2842,
570 doi:[10.5194/acp-22-2817-2022](https://doi.org/10.5194/acp-22-2817-2022), 2022.

571 Ludemann, C. I., Gruere, A., Heffer, P. and Dobermann, A.: Global data on fertilizer use by crop and
572 by country, *Sci. Data*, 9(1), 501, doi:[10.1038/s41597-022-01592-z](https://doi.org/10.1038/s41597-022-01592-z), 2022.

573 Malm, W. C., Johnson, C. E., and Bresch, J. F.: Application of principal component analysis for purpose
574 of identifying source receptor relationships, in *Receptor Methods for Source Apportionment*, Pace,
575 T.G., Ed.; Publication TR-5, Air Pollution Control Association, Pittsburgh, PA, pp. 127–148, 1986.

576 Marais, E. A., Pandey, A. K., Van Damme, M., Clarisse, L., Coheur, P.-F., Shephard, M. W., Cady-Pereira,
577 K. E., Misselbrook, T., Zhu, L., Luo, G. and Yu, F.: UK Ammonia Emissions Estimated With Satellite

578 Observations and GEOS-Chem, *J. Geophys. Res. Atmos.*, 126(18), e2021JD035237,
579 doi:<https://doi.org/10.1029/2021JD035237>, 2021.

580 Martino, M., Tassone, A., Angiuli, L., Naccarato, A., Dambruoso, P. R., Mazzone, F., Trizio, L., Leonardi,
581 C., Petracchini, F., Sprovieri, F., Pirrone, N., D'Amore, F. and Bencardino, M.: First atmospheric mercury
582 measurements at a coastal site in the Apulia region: seasonal variability and source analysis, *Environ.*
583 *Sci. Pollut. Res.*, 29(45), 68460–68475, doi:10.1007/s11356-022-20505-6, 2022.

584 McDuffie, E. E., Smith, S. J., O'Rourke, P., Tibrewal, K., Venkataraman, C., Marais, E. A., Zheng, B.,
585 Crippa, M., Brauer, M., and Martin, R. V.: A global anthropogenic emission inventory of atmospheric
586 pollutants from sector- and fuel-specific sources (1970–2017): an application of the Community
587 Emissions Data System (CEDS), *Earth Syst. Sci. Data*, 12, 3413–3442, [https://doi.org/10.5194/essd-12-](https://doi.org/10.5194/essd-12-3413-2020)
588 [3413-2020](https://doi.org/10.5194/essd-12-3413-2020), 2020.

589 Nair, A. A. and Yu, F.: Quantification of Atmospheric Ammonia Concentrations: A Review of Its
590 Measurement and Modeling, *Atmosphere (Basel)*, 11(10), doi:10.3390/atmos11101092, 2020.

591 Osada, K.: Measurement report: Short-term variation in ammonia concentrations in an urban area
592 increased by mist evaporation and emissions from a forest canopy with bird droppings, *Atmos. Chem.*
593 *Phys.*, 20, 11941–11954, <https://doi.org/10.5194/acp-20-11941-2020>, 2020.

594 Pazmiño, A., Beekmann, M., Goutail, F., Ionov, D., Bazureau, A., Nunes-Pinharanda, M., Hauchecorne,
595 A., and Godin-Beekmann, S.: Impact of the COVID-19 pandemic related to lockdown measures on
596 tropospheric NO₂ columns over Île-de-France, *Atmos. Chem. Phys.*, 21, 18303–18317,
597 <https://doi.org/10.5194/acp-21-18303-2021>, 2021.

598 Perrino, C., Catrambone, M., Di Menno Di Bucchianico, A. and Allegrini, I.: Gaseous ammonia in the
599 urban area of Rome, Italy and its relationship with traffic emissions, *Atmos. Environ.*, 36(34), 5385–
600 5394, doi:[https://doi.org/10.1016/S1352-2310\(02\)00469-7](https://doi.org/10.1016/S1352-2310(02)00469-7), 2002.

601 Petetin, H., et al.: Assessing the ammonium nitrate formation regime in the Paris megacity and its
602 representation in the CHIMERE model, *Atmos. Chem. Phys.*, 16, 10419-10440, doi:10.5194/acp-16-
603 10419-2016, 2016.

604 Petit, J.-E., Favez, O., Sciare, J., Crenn, V., Sarda-Estève, R., Bonnaire, N., Močnik, G., Dupont, J.-C.,
605 Haefelin, M., and Leoz-Garziandia, E.: Two years of near real-time chemical composition of submicron
606 aerosols in the region of Paris using an Aerosol Chemical Speciation Monitor (ACSM) and a multi-
607 wavelength Aethalometer, *Atmos. Chem. Phys.*, 15, 2985–3005, [https://doi.org/10.5194/acp-15-](https://doi.org/10.5194/acp-15-2985-2015)
608 [2985-2015](https://doi.org/10.5194/acp-15-2985-2015), 2015.

609 Pu, W., Sheng, J., Tian, P., Huang, M., Liu, X., Collett, J. L., Li, Z., Zhao, X., He, D., Dong, F., Zhang, N.,
610 Quan, W., Qiu, Y., Song, Y., Lin, W., Pan, Y. and Ma, Z.: On-road mobile mapping of spatial variations
611 and source contributions of ammonia in Beijing, China, *Sci. Total Environ.*, 864, 160869,
612 doi:<https://doi.org/10.1016/j.scitotenv.2022.160869>, 2023.

613 Pope III, C. A., et al.: Fine-particulate air pollution and life expectancy in the United States, *N. Engl. J.*
614 *Med.*, 360(4), 376–386, doi:10.1056/NEJMsa0805646, 2009.

615 Qadri, A. M., Singh, G. K., Paul, D., Gupta, T., Rabha, S., Islam, N. and Saikia, B. K.: Variabilities of $\delta^{13}\text{C}$
616 and carbonaceous components in ambient PM_{2.5} in Northeast India: Insights into sources and

617 atmospheric processes, Environ. Res., 214, 113801,
618 doi:<https://doi.org/10.1016/j.envres.2022.113801>, 2022.

619 Ren, B., Xie, P., Xu, J., Li, A., Tian, X., Hu, Z., Huang, Y., Li, X., Zhang, Q., Ren, H. and Ji, H.: Use of the
620 PSCF method to analyze the variations of potential sources and transports of NO₂, SO₂, and HCHO
621 observed by MAX-DOAS in Nanjing, China during 2019, *Sci. Total Environ.*, 782, 146865,
622 doi:<https://doi.org/10.1016/j.scitotenv.2021.146865>, 2021.

623 Rockström, J., Steffen, W., Noone, K., Persson, Å., Chapin, F. S., Lambin, E. F., Lenton, T. M., Scheffer,
624 M., Folke, C., Schellnhuber, H. J., Nykvist, B., de Wit, C. A., Hughes, T., van der Leeuw, S., Rodhe, H.,
625 Sörlin, S., Snyder, P. K., Costanza, R., Svedin, U., Falkenmark, M., Karlberg, L., Corell, R. W., Fabry, V. J.,
626 Hansen, J., Walker, B., Liverman, D., Richardson, K., Crutzen, P. and Foley, J. A.: A safe operating space
627 for humanity, *Nature*, 461(7263), 472–475, doi:[10.1038/461472a](https://doi.org/10.1038/461472a), 2009.

628 Roe, S.; Spivey, M.; Lindquist, H.; Thesing, K.; Strait, R.; Pechan, E.; Associates, I. Estimating Ammonia
629 Emissions from Anthropogenic Nonagricultural Sources. EPA Emission Inventory Improvement
630 Program. Technical Report; Emission Inventory Improvement Program, 2004.

631 Shephard, M.W., and Cady-Pereira, K.E.: Cross-track Infrared Sounder (CrIS) satellite observations of
632 tropospheric ammonia, *Atmos. Meas. Tech.*, 8, 1323-1336, 2015.

633 Sintermann, J., Dietrich, K., Häni, C., Bell, M., Jocher, M. and Neftel, A.: A miniDOAS instrument
634 optimised for ammonia field measurements, *Atmos. Meas. Tech.*, 9(6), 2721–2734, doi:[10.5194/amt-9-2721-2016](https://doi.org/10.5194/amt-9-2721-2016), 2016.

636 Stein, A. F., Draxler, R. R., Rolph, G. D., Stunder, B. J. B., Cohen, M. D. and Ngan, F.: NOAA’s HYSPLIT
637 Atmospheric Transport and Dispersion Modeling System, *Bull. Am. Meteorol. Soc.*, 96(12), 2059–2077,
638 doi:[10.1175/BAMS-D-14-00110.1](https://doi.org/10.1175/BAMS-D-14-00110.1), 2015.

639 Sudesh, S, and Kulshrestha, U. C. Diurnal Variation of Ambient NH₃ in Relation with Agricultural
640 Activities and Meteorological Factors at a Rural Site in North India. *Curr World Environ*, S11.
641 DOI:<http://dx.doi.org/10.12944/CWE.16.Special-Issue1.02>, 2021.

642 Sun, K., Tao, L., Miller, D. J., Pan, D., Golston, L. M., Zondlo, M. A., Griffin, R. J., Wallace, H. W., Leong,
643 Y. J., Yang, M. M., Zhang, Y., Mauzerall, D. L. and Zhu, T.: Vehicle Emissions as an Important Urban
644 Ammonia Source in the United States and China, *Environ. Sci. Technol.*, 51(4), 2472–2481,
645 doi:[10.1021/acs.est.6b02805](https://doi.org/10.1021/acs.est.6b02805), 2017.

646 Sutton, M. A., Reis, S., Riddick, S. N., Dragosits, U., Nemitz, E., Theobald, M. R., Tang, Y. S., Braban, C.
647 F., Vieno, M., Dore, A. J., Mitchell, R. F., Wanless, S., Daunt, F., Fowler, D., Blackall, T. D., Milford, C.,
648 Flechard, C. R., Loubet, B., Massad, R., Cellier, P., Personne, E., Coheur, P. F., Clarisse, L., Van Damme,
649 M., Ngadi, Y., Clerbaux, C., Skjøth, C. A., Geels, C., Hertel, O., Wichink Kruit, R. J., Pinder, R. W., Bash, J.
650 O., Walker, J. T., Simpson, D., Horváth, L., Misselbrook, T. H., Bleeker, A., Dentener, F. and de Vries, W.:
651 Towards a climate-dependent paradigm of ammonia emission and deposition, *Philos. Trans. R. Soc.
652 Lond. B. Biol. Sci.*, 368(1621), 20130166, doi:[10.1098/rstb.2013.0166](https://doi.org/10.1098/rstb.2013.0166), 2013.

653 Sutton, M.; Dragosits, U.; Tang, Y.; Fowler, D.: Ammonia emissions from nonagricultural sources in the
654 UK. *Atmos. Environ.* 34, 855– 869, DOI: [10.1016/S1352-2310\(99\)00362-3](https://doi.org/10.1016/S1352-2310(99)00362-3), 2000.

655 Twigg, M. M., Berkhout, A. J. C., Cowan, N., Crunaire, S., Dammers, E., Ebert, V., Gaudion, V., Haaima,
656 M., Häni, C., John, L., Jones, M. R., Kamps, B., Kentisbeer, J., Kupper, T., Leeson, S. R., Leuenberger, D.,

657 Lüttschwager, N. O. B., Makkonen, U., Martin, N. A., Missler, D., Mounsor, D., Neftel, A., Nelson, C.,
658 Nemitz, E., Oudwater, R., Pascale, C., Petit, J.-E., Pogany, A., Redon, N., Sintermann, J., Stephens, A.,
659 Sutton, M. A., Tang, Y. S., Zijlmans, R., Braban, C. F., and Niederhauser, B.: Intercomparison of in situ
660 measurements of ambient NH₃: instrument performance and application under field conditions,
661 *Atmos. Meas. Tech.*, 15, 6755–6787, <https://doi.org/10.5194/amt-15-6755-2022>, 2022.

662 Van Damme, M., Clarisse, L., Stavrakou, T., Wichink Kruit, R., Sellekaerts, L., Viatte, C., Clerbaux, C. and
663 Coheur, P.-F.: On the weekly cycle of atmospheric ammonia over European agricultural hotspots, *Sci.*
664 *Rep.*, 12(1), 12327, doi:10.1038/s41598-022-15836-w, 2022.

665 Van Damme, M., Clarisse, L., Franco, B., Sutton, M. A., Erisman, J. W., Wichink Kruit, R., van Zanten,
666 M., Whitburn, S., Hadji-Lazaro, J., Hurtmans, D., Clerbaux, C., & Coheur, P.-F.: Global, regional and
667 national trends of atmospheric ammonia derived from a decadal (2008–2018) satellite record.
668 *Environmental Research Letters*, 16(5), 55017. <https://doi.org/10.1088/1748-9326/abd5e0>, 2021.

669 Van Damme, M., Clarisse, L., Whitburn, S., Hadji-Lazaro, J., Hurtmans, D., Clerbaux, C. and Coheur, P.-
670 F.: Industrial and agricultural ammonia point sources exposed, *Nature*, 564(7734), 99–103,
671 doi:10.1038/s41586-018-0747-1, 2018.

672 Van Damme, M., Clarisse, L., Dammers, E., Liu, X., Nowak, J. B., Clerbaux, C., Flechard, C. R., Galy-
673 Lacaux, C., Xu, W., Neuman, J. A., Tang, Y. S., Sutton, M. A., Erisman, J. W. and Coheur, P. F.: Towards
674 validation of ammonia (NH₃) measurements from the IASI satellite, *Atmos. Meas. Tech.*, 8(3), 1575–
675 1591, doi:10.5194/amt-8-1575-2015, 2015.

676 Viatte, C. (2023). NH₃ from Mini Doas [Data set]. LATMOS.

677 Viatte, C., Abeed, R., Yamanouchi, S., Porter, W. C., Safieddine, S., Van Damme, M., Clarisse, L., Herrera,
678 B., Grutter, M., Coheur, P.-F., Strong, K. and Clerbaux, C.: NH₃ spatiotemporal variability over Paris,
679 Mexico City, and Toronto, and its link to PM_{2.5} during pollution events, *Atmos. Chem. Phys.*, 22(19),
680 12907–12922, doi:10.5194/acp-22-12907-2022, 2022.

681 Viatte, C., Petit, J.-E., Yamanouchi, S., Van Damme, M., Doucerain, C., Germain-Piaulenne, E., Gros, V.,
682 Favez, O., Clarisse, L., Coheur, P.-F., Strong, K. and Clerbaux, C.: Ammonia and PM_{2.5} air pollution in
683 paris during the 2020 covid lockdown, *Atmosphere*, 12(2), doi:10.3390/atmos12020160, 2021.

684 Viatte, C., Wang, T., Van Damme, M., Dammers, E., Meleux, F., Clarisse, L., Shephard, M. W., Whitburn,
685 S., François Coheur, P., Cady-Pereira, K. E. and Clerbaux, C.: Atmospheric ammonia variability and link
686 with particulate matter formation: A case study over the Paris area, *Atmos. Chem. Phys.*, 20(1),
687 doi:10.5194/acp-20-577-2020, 2020.

688 Volten, H., Bergwerff, J. B., Haaima, M., Lolkema, D. E., Berkhout, A. J. C., van der Hoff, G. R., Potma,
689 C. J. M., Wichink Kruit, R. J., van Pul, W. A. J. and Swart, D. P. J.: Two instruments based on differential
690 optical absorption spectroscopy (DOAS) to measure accurate ammonia concentrations in the
691 atmosphere, *Atmos. Meas. Tech.*, 5(2), 413–427, doi:10.5194/amt-5-413-2012, 2012.

692 von Bobruzki, K., Braban, C. F., Famulari, D., Jones, S. K., Blackall, T., Smith, T. E. L., Blom, M., Coe, H.,
693 Gallagher, M., Ghalaieny, M., McGillen, M. R., Percival, C. J., Whitehead, J. D., Ellis, R., Murphy, J.,
694 Mohacsi, A., Pogany, A., Junninen, H., Rantanen, S., Sutton, M. A. and Nemitz, E.: Field inter-

695 comparison of eleven atmospheric ammonia measurement techniques, *Atmos. Meas. Tech.*, 3(1), 91–
696 112, doi:10.5194/amt-3-91-2010, 2010.

697 Wang, B., Liu, Z., Li, Z., Sun, Y., Wang, C., Zhu, C., Sun, L., Yang, N., Bai, G., Fan, G., Sun, X., Xia, Z., Pan,
698 G., Xu, C. and Yan, G.: Characteristics, chemical transformation and source apportionment of volatile
699 organic compounds (VOCs) during wintertime at a suburban site in a provincial capital city, east China,
700 *Atmos. Environ.*, 298, 119621, doi:https://doi.org/10.1016/j.atmosenv.2023.119621, 2023.

701 Wang, S., Nan, J., Shi, C., Fu, Q., Gao, S., Wang, D., Cui, H., Saiz-Lopez, A. and Zhou, B.: Atmospheric
702 ammonia and its impacts on regional air quality over the megacity of Shanghai, China, *Sci. Rep.*, 5(1),
703 15842, doi:10.1038/srep15842, 2015.

704 Wang, Y.Q., Zhang, X.Y. and Draxler, R.:TrajStat: GIS-based software that uses various trajectory
705 statistical analysis methods to identify potential sources from long-term air pollution measurement
706 data. *Environmental Modelling & Software*, 24: 938-939, 2009.

707 Warner, J. X., Wei, Z., Strow, L. L., Dickerson, R. R., and Nowak, J. B.: The global tropospheric ammonia
708 distribution as seen in the 13-year AIRS measurement record, *Atmos. Chem. Phys.*, 16, 5467-5479,
709 https://doi.org/10.5194/acp-16-5467-2016, 2016.

710 Wen, Y., Zhang, S., Wu, Y. and Hao, J.: Vehicular ammonia emissions: An underappreciated emission
711 source in densely-populated areas, *Atmos. Chem. Phys. Discuss.*, 2022, 1–14, doi:10.5194/acp-2022-
712 828, 2022.

713 Whitehead, J., Longley, D., Coe, H. and Gallagher, M.: Hourly concentrations of ammonia during the
714 winter in Manchester, UK, related to traffic and background sources, Fifth Conference on Urban
715 Environment, Session 14 urban air quality (including urban airshed modeling and urban air chemistry
716 experiments), Vancouver BC, Canada, 23-26 August 2004.

717 Zachary, M., Yin, L. and Zacharia, M.: Application of PSCF and CWT to Identify Potential Sources of
718 Aerosol Optical Depth in ICIPE Mbita. *Open Access Library Journal*, 5, 1-12. doi: 10.4236/oalib.1104487,
719 2018.

720 Zhang, Q., Wei, N., Zou, C. and Mao, H.: Evaluating the ammonia emission from in-use vehicles using
721 on-road remote sensing test, *Environ. Pollut.*, 271, 116384,
722 doi:https://doi.org/10.1016/j.envpol.2020.116384, 2021.